Supplementary information

Scalable Production of Foam-like Nickel-Molybdenum Coatings via Plasma Spraying as Bifunctional Electrocatalysts for Water Splitting

Xiuyu Wu,[1] Alexis Piñeiro García,[1] Mouna Rafei,[1] Nicolas Boulanger,[1] Esdras Josué Canto-Aguilar, and Eduardo Gracia-Espino.[1]

[1] *Department of Physics, Umeå University, SE-901 87 Umeå, Sweden.*

*Corresponding author: Eduardo Gracia-Espino (eduardo.gracia@umu.se)

Table S1. Spraying parameters and sample labels for samples tested for HER and OER.

Current (A)	**Primary gas (NL min^{-1})**	**Secondary gas (NL min^{-1})**	**Power (kW)**	**Spray distance (mm)**	**Sample label**	
500	35	0.5	20	250	NiMo 20kW@250mm	HER
600	35	0.5	24	250	NiMo 24kW@250mm	HER
750	50	2	38	250	NiMo 38kW@250mm	HER
500	35	0.5	20	200	NiMo 20kW@200mm	HER
500	35	0.5	20	250	NiMo 20kW@250mm	HER
500	35	0.5	20	300	NiMo 20kW@300mm	HER
400	20	0.5	16	100	NiMo 16kW@100mm	OER
400	20	0.5	16	150	NiMo 16kW@150mm	OER
400	35	0.5	17	100	NiMo 17kW@100mm	OER

Table S2. Double-layer capacitance calculated from CV obtained for three replicates of the sample NiMo 20kW@100mm in a solution 0.1 M NBu_4PF_6 in CH_3CN, before and after the Al leaching. The similar values of the capacitance calculated either with the cathodic or the anodic currents indicate a high coulombic efficiency and reproducibility of the measurements.

	Before Al leaching		After Al leaching	
n	$C_{cathodic}$ (F cm^{-2})	C_{anodic} (F cm^{-2})	$C_{cathodic}$ (F cm^{-2})	C_{anodic} (F cm^{-2})
1	0.0032	0.0031	0.0138	0.0146
2	0.003	0.0027	0.0132	0.0142
3	0.0035	0.0031	0.0155	0.016
Average ($\bar{x}$)	0.0032	0.0030	0.0142	0.0149
Std. Deviation (σ)	0.0003	0.0002	0.0012	0.0009
Coefficient of variation (Cv)	9.4 %	6.7%	8.4%	6.0%

Table S3. Catalysts loading per square centimetre for samples sprayed at 20 kW but different distances (weighted area 1 × 4 cm). Electrochemically active surface area (ECSA), and overpotential needed to achieve a current density of -50 mA cm^{-2}.

Sample Label	Weight (mg cm^{-2})	ECSA (cm^2 per cm^2 of geometric area)	η_{50} (mV)
NiMo 20kW@100mm	200	1768.84	42
NiMo 20kW@200mm	126	1065.72	46
NiMo 20kW@250mm	90	573.58	62
NiMo 20kW@300mm	78	455.38	88

Table S4. Comparison of mass activity for different noble-metal free electrocatalysts for HER in 1 M KOH.

Catalyst	Overpotential (mV)	Mass activity (A g^{-1})	Reference.
NiMo 20kW@100mm	**100**	**0.65**	**This work**
Ni nanoparticles	50	0.28	[1]
3D-printed NiMo	100	0.32	[2]
Ni-Mo	200	0.28	[3]
Co Single-Atom-Catalyst	100	2.9	[4]
Co NPs	100	0.80	[4]
3D $NiCu_{ed}$	-	0.24	[5]
$MoSe_2$–$NiSe_2$–$CoSe_2$/PNCF	100	0.19	[6]
Mo-NiS/Ni_3S_2-0.08 S	100	0.15	[7]
MoS_2/Ni	100	1.4	[8]

Table S5. Comparison of mass activity for different noble-metal free electrocatalysts for OER in 1 M alkaline electrolyte (KOH or NaOH).

Catalyst	Overpotential (mV)	Mass activity (A g^{-1})	Reference.
NiMo 16kW@100mm	**300**	**0.3**	**This work**
SCoNC	310	0.278	[9]
FeCo nanoparticles	310	0.3	[10]
NiFe LDH/Cu(OH)2/Cu	370	0.153	[11]
Cu(OH)2/Cu	370	0.044	[11]
Co3O4/Co0.85Se/Co9Se8	300	0.29	[12]
Co0.5Ni0.5Fe2O4	300	119	[13]
NCoM-Cb-Ar	500	536.5	[14]

Table S6. Value of the resistors used in the equivalent circuit model shown in **Figure 10e** (main manuscript) after fitting the Nyquist plots (**Figure 10e**) at different applied potentials.

Potential (V vs. RHE)	R_1 (Ω)	R_2 (Ω)	R_3 (Ω)
1.436	0.42	0.36	17.59
1.461	0.40	0.31	4.92
1.486	0.40	0.22	1.03
1.511	0.40	0.36	0.20

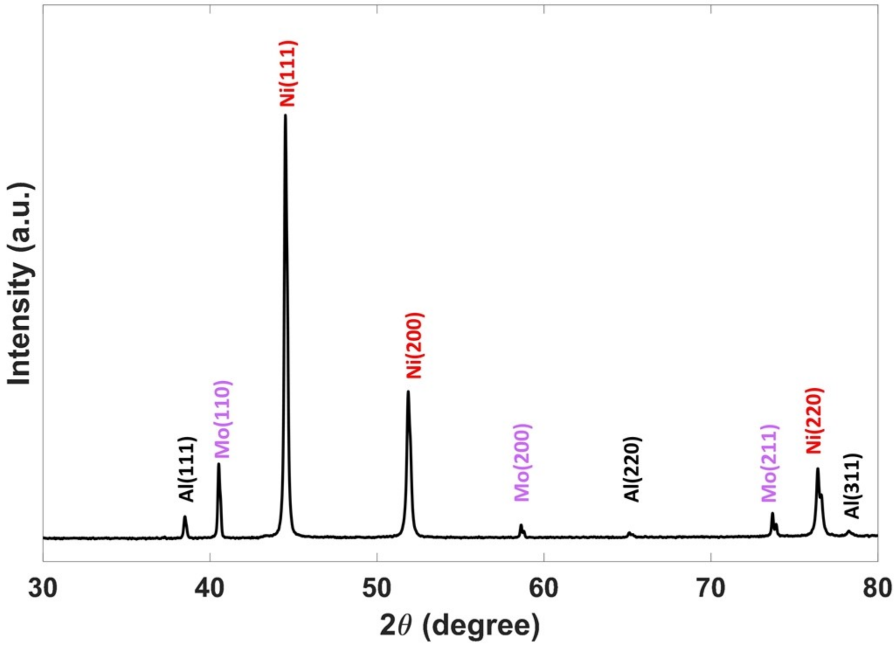

Figure S1. *X-ray diffractogram of the initial powder showing features corresponding to individual Ni, Al, and Mo. No signs of Ni-Mo alloys were observed.*

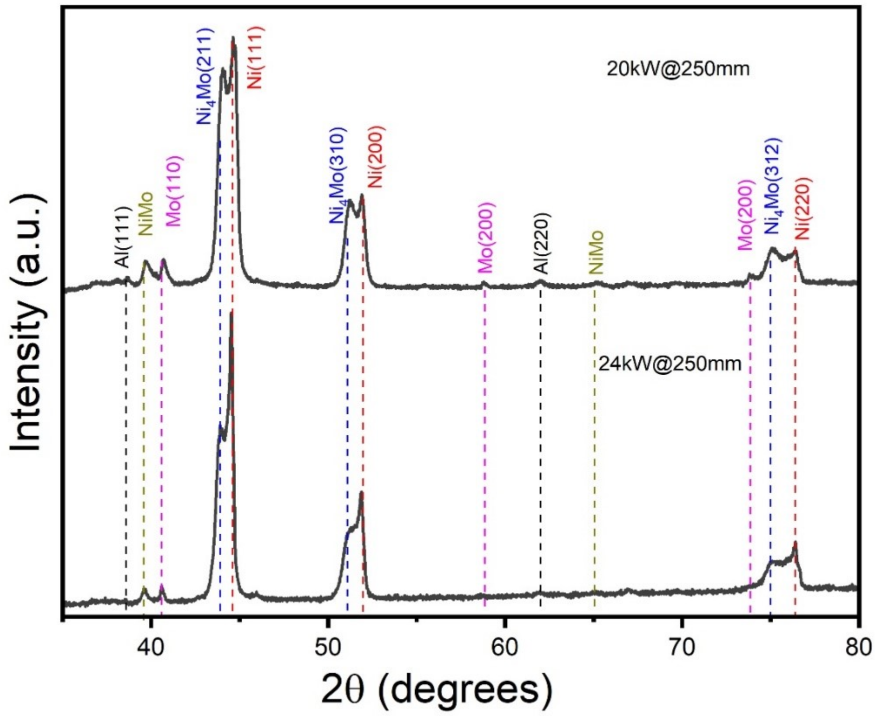

Figure S2. *XRD patterns of as-sprayed NiAlMo coatings at 250 mm distance and two different power values.*

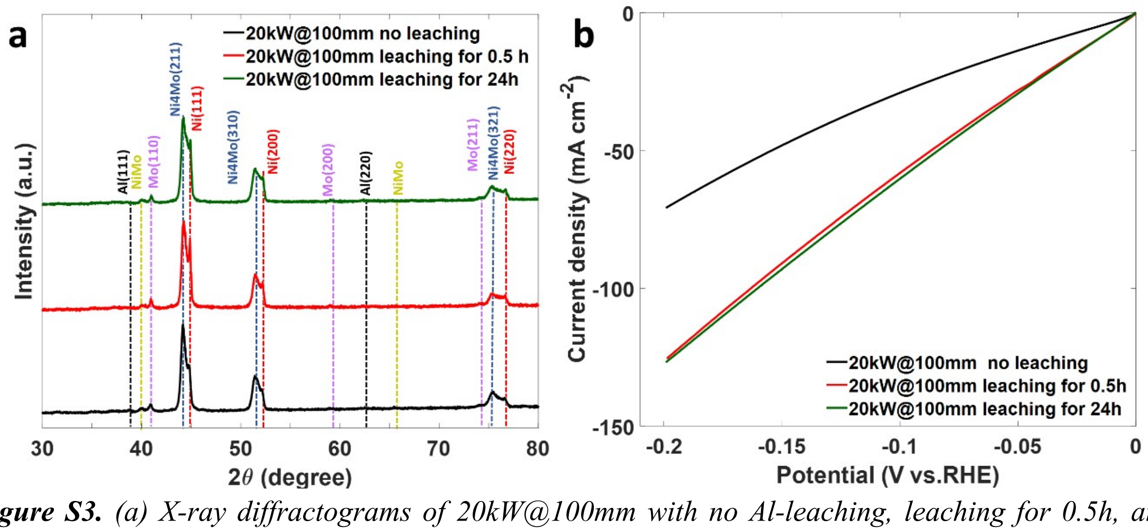

Figure S3. *(a) X-ray diffractograms of 20kW@100mm with no Al-leaching, leaching for 0.5h, and leaching for 24h. (b) Polarization curves of the electrodes in (a) without iR-correction.*

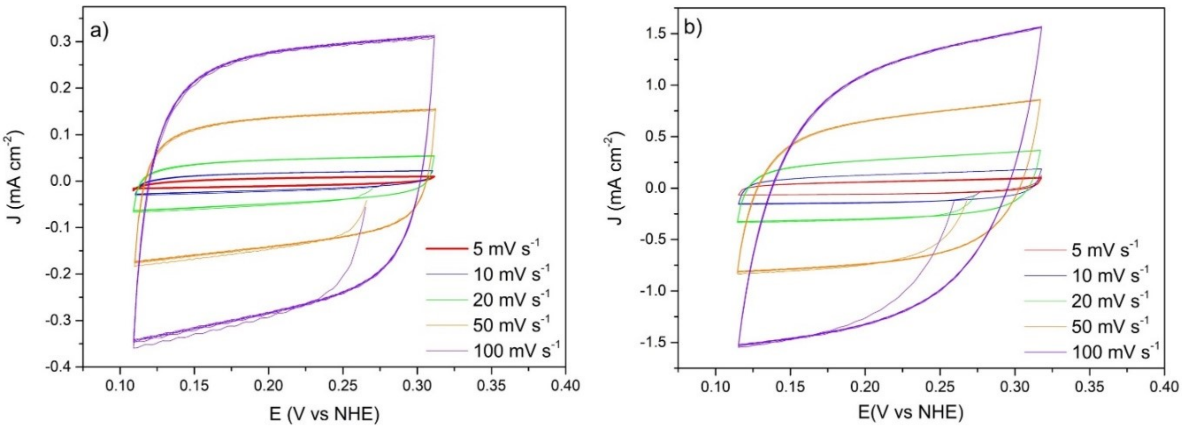

Figure S4. *Cyclic voltammograms for NiMo 20kW@100mm coatings in a three electrode-electrochemical cell. (a)* ***Before*** *and (b)* ***after Al leaching***. *The measurements were performed using a working solution consisting of 0.1 M NBu_4PF_6 in CH_3CN (saturated with Ar), Ag/Ag^+ (0.1 NBu_4PF_6, 0.01 M $AgNO_3$) as reference electrode (0.54 V vs NHE), a Pt-wire as counter electrode and varying the scan rate from 5 to 100 mV s^{-1}.*

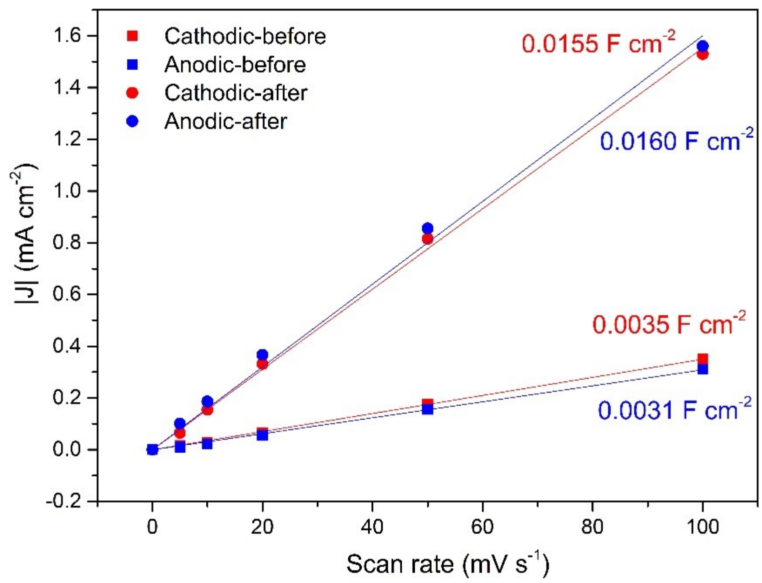

Figure S5. *Double-layer capacitance for the electrodes* ***before and after Al leaching*** *calculated with the cathodic (0.114 V vs NHE) and anodic currents (0.317 V vs NHE) at different scan rates from the voltammograms in* ***Figure S4***. *The similar currents observed in the cathodic and anodic sweeps indicate a high Coulombic efficiency of the charging/discharging processes at the electrode surface/electrolyte interface.*

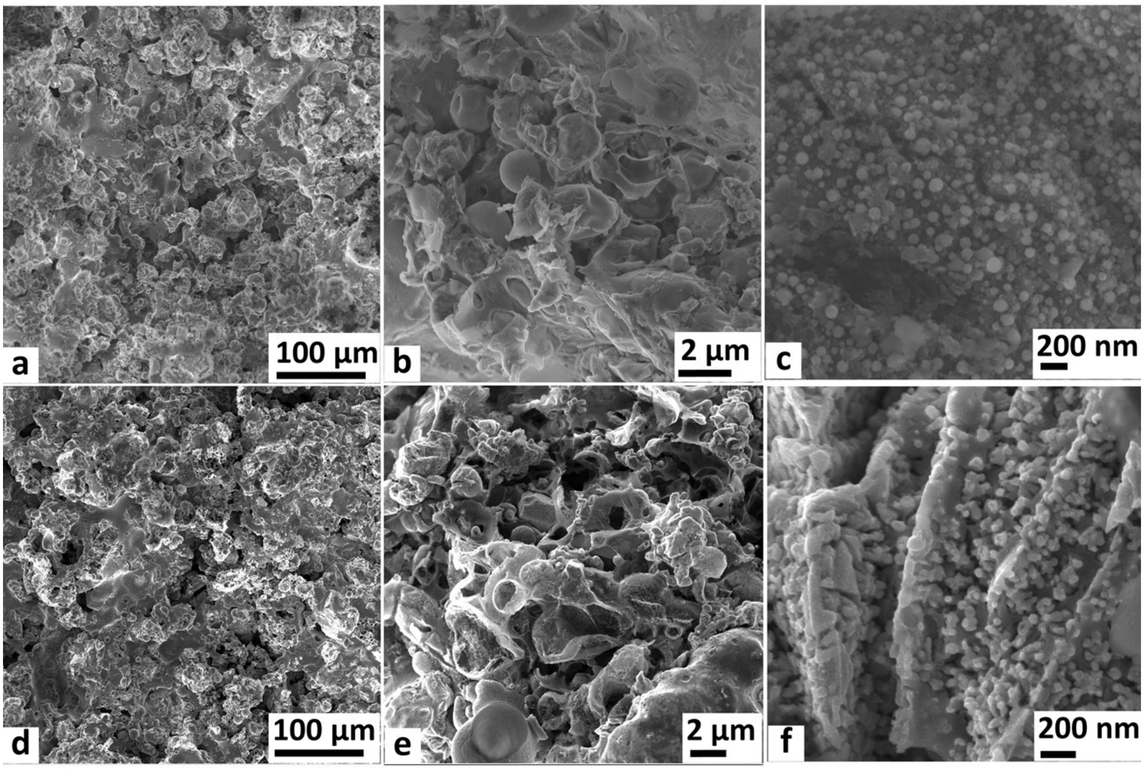

Figure S6. *SEM images of NiMo 20kW@100mm sample (a-c) as-sprayed, and (d-f) after Al leaching.*

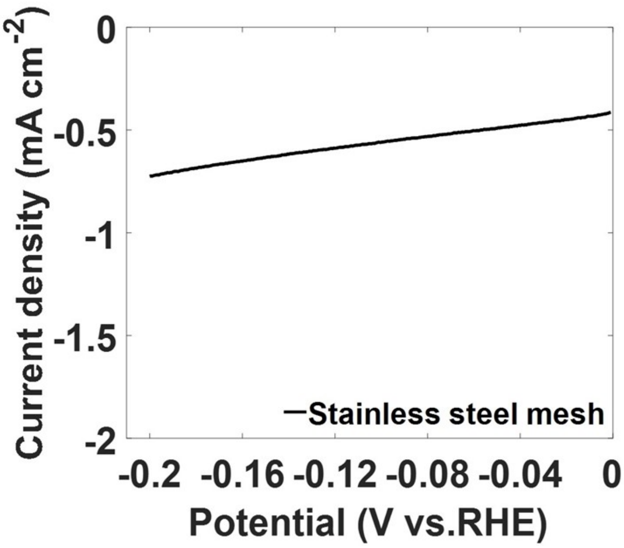

Figure S7. *Polarization curve of stainless-steel mesh in the potential range relevant for the HER.*

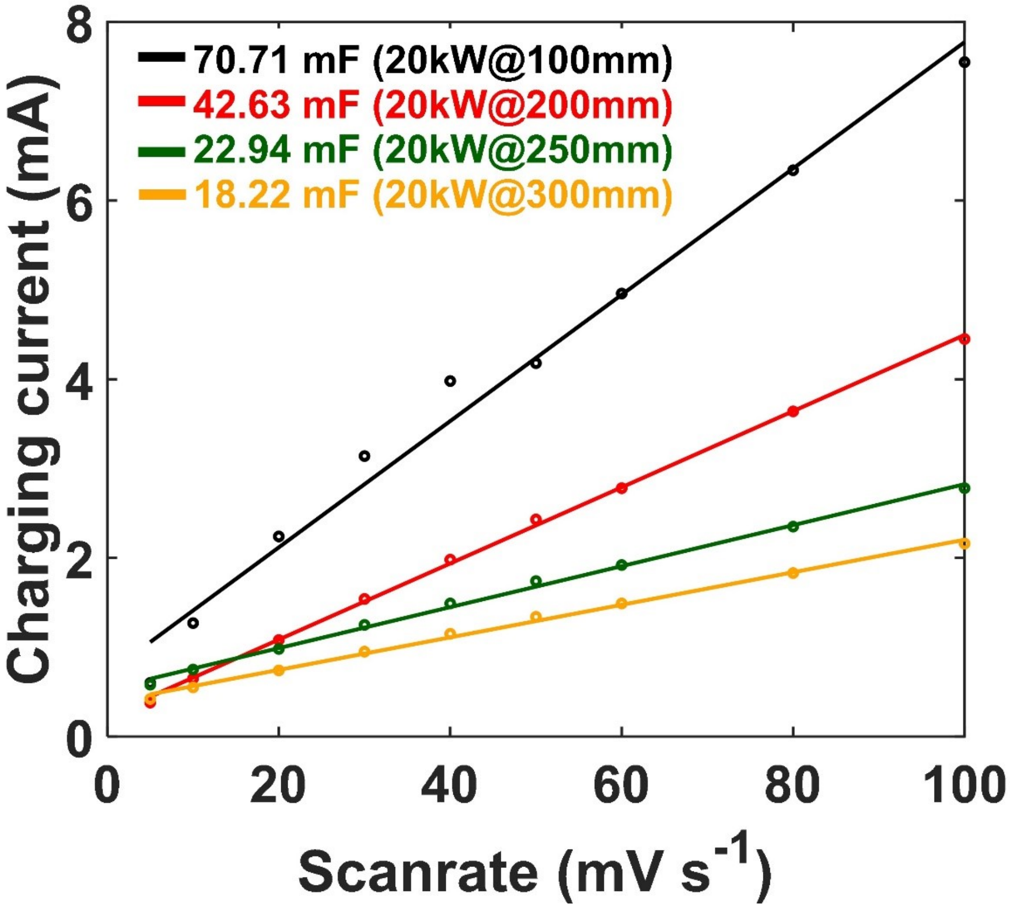

Figure S8. *Double layer capacitance measurements of NiMo samples sprayed at 20kW at different distances. The electrochemical surface area (ECSA) was calculated using ECSA = C_{dl}/40 µF cm^{-2}, where 40 µF cm^{-2} is the charge density for a flat surface. The samples had an exposed geometric area of 1 cm^2. The observed ECSA are 1768.84 cm^2(20kW@100mm), 1065.72 cm^2 (20kW@200mm), 573.58 cm^2 (20kW@250mm), and 455.38 cm^2 (20kW@300mm).*

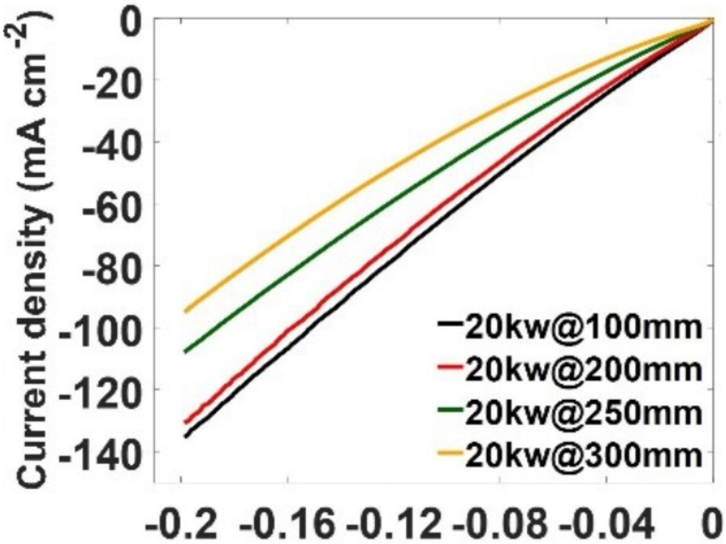

Figure S9. *Polarization curves of NiMo 20kW@100mm, 20kW@200mm, 20kW@250mm, and 20kW@300mm before iR-correction.*

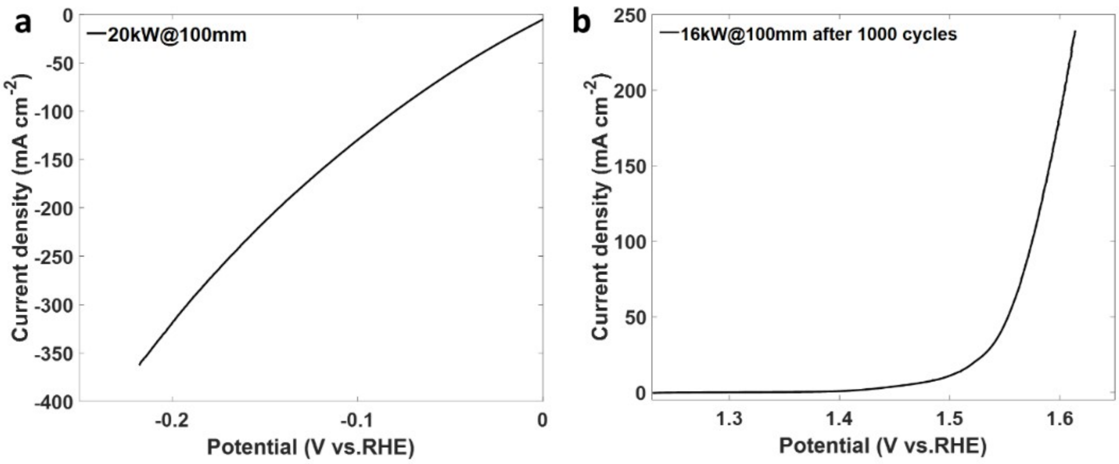

Figure S10. *(a) iR-corrected polarization curve of 20kW@100mm measured up to -0.5 V vs RHE. (b) iR-corrected polarization curve of 16kW@100mm measured up to 1.83 V vs RHE after activation (1000 CVs).*

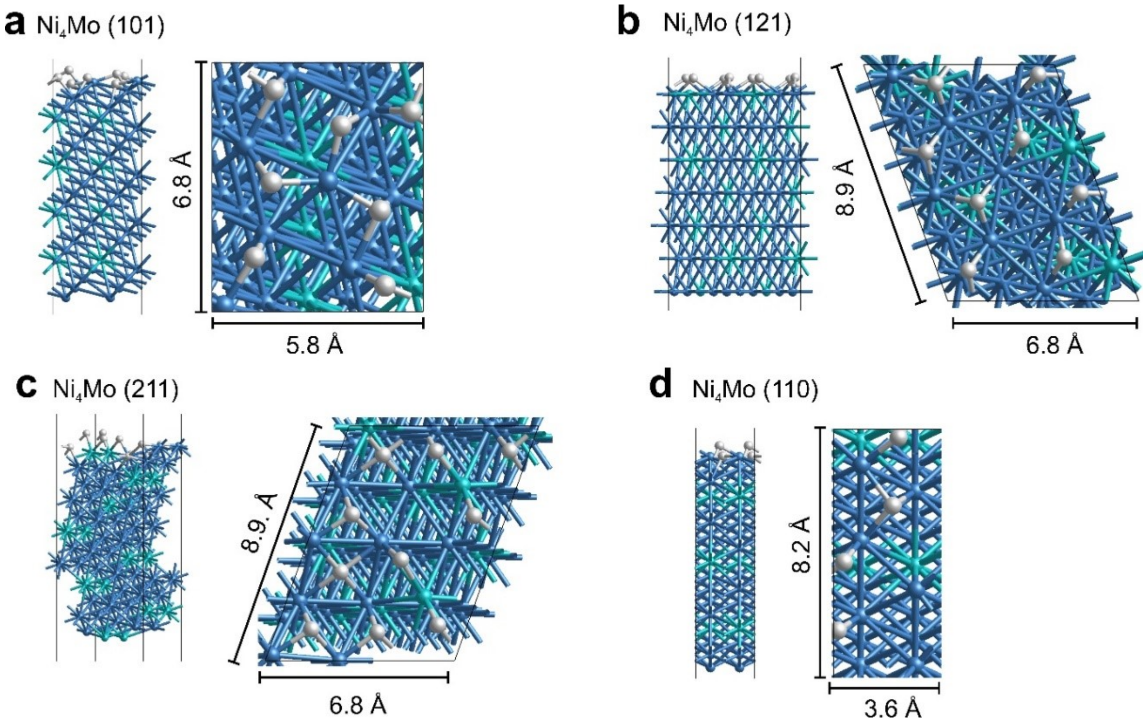

Figure S11. *Atomic models used to evaluate the hydrogen adsorption free energy of Ni_4Mo. (a-d) (101), (121), (211), and (110) surface. The adsorption energy was calculated at full hydrogen monolayer with the hydrogen atoms sitting at 3-fold fcc sites as expected for Ni-based alloys.*

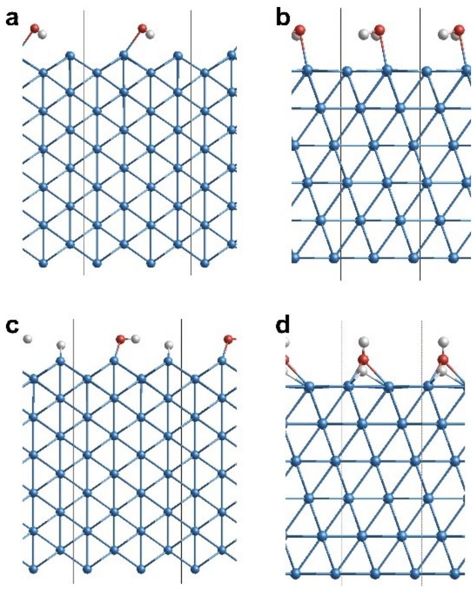

Figure S12. *(a-b) Water adsorption on (101) and (111) surfaces of Ni. (c-d) Water dissociation into H and OH on (101) and (111) Ni surface. The dissociation energy (E_{diss}) is evaluated as $E_{diss} = E_{H\text{-}OH\text{-}surf} - E_{H2O\text{-}surf}$, where $E_{H\text{-}OH\text{-}surf}$ ($E_{H2O\text{-}surf}$) is the energy of the H and OH (H_2O) adsorbed onto the Ni surface. E_{diss} for Ni (101), and Ni(111) is -0.89 and -0.40 eV, respectively. $E_{diss} < 0$ indicates favourable configuration.*

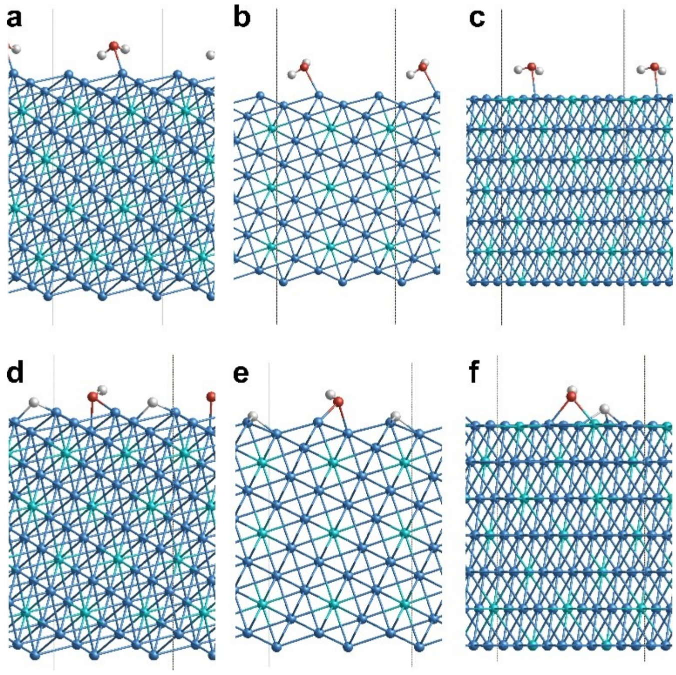

Figure S13. *(a-c) Water adsorption on (101), (110), and (121) surfaces of* Ni_4Mo*. (d-f) Water dissociation into H and OH on (101), (110), and (121) surfaces of* Ni_4Mo*. The dissociation energy* (E_{diss}) *is evaluated as* $E_{diss} = E_{H\text{-}OH\text{-}surf} - E_{H2O\text{-}surf}$*, where* $E_{H\text{-}OH\text{-}surf}$ ($E_{H2O\text{-}surf}$) *is the energy of the H and OH* (H_2O) *adsorbed onto the* Ni_4Mo *surface.* E_{diss} *for (101), (110), and (121) is -0.51, -0.96, and -1.16 eV, respectively.* $E_{diss} < 0$ *indicates favourable configuration.*

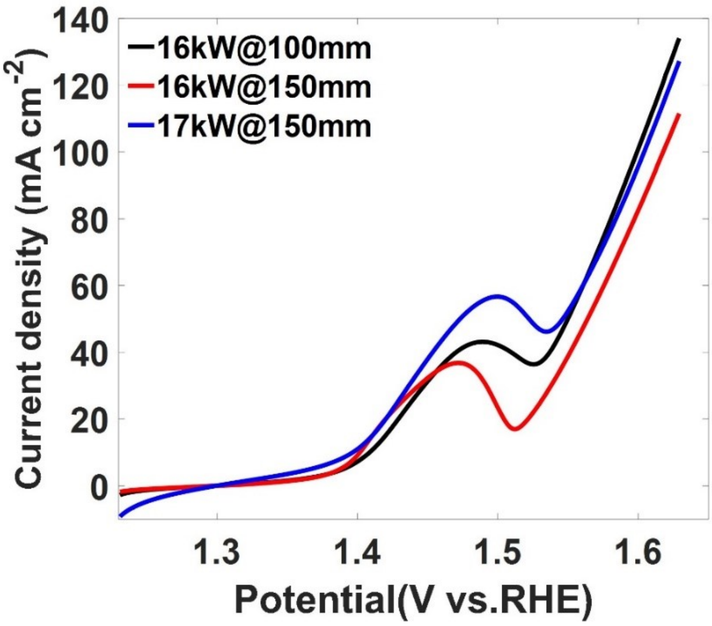

Figure S14. *Polarization curves of NiMo 16kW@100mm, NiMo 16kW@150mm, and NiMo 17kW@150mm after 1000 CVs activation process, the polarization curves were recorded at a scan rate of 5 mV* s^{-1}*.*

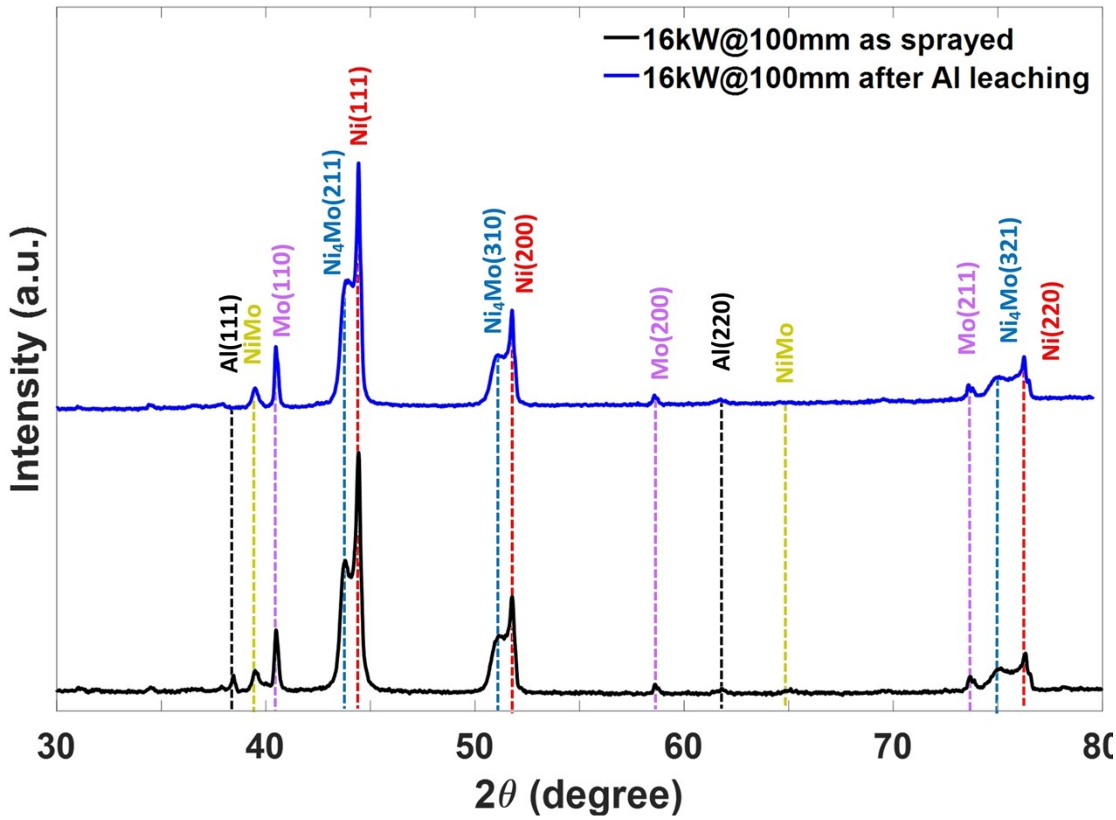

Figure S15. *X-ray diffractograms of NiMo 16kW@100mm as sprayed and after Al leaching.*

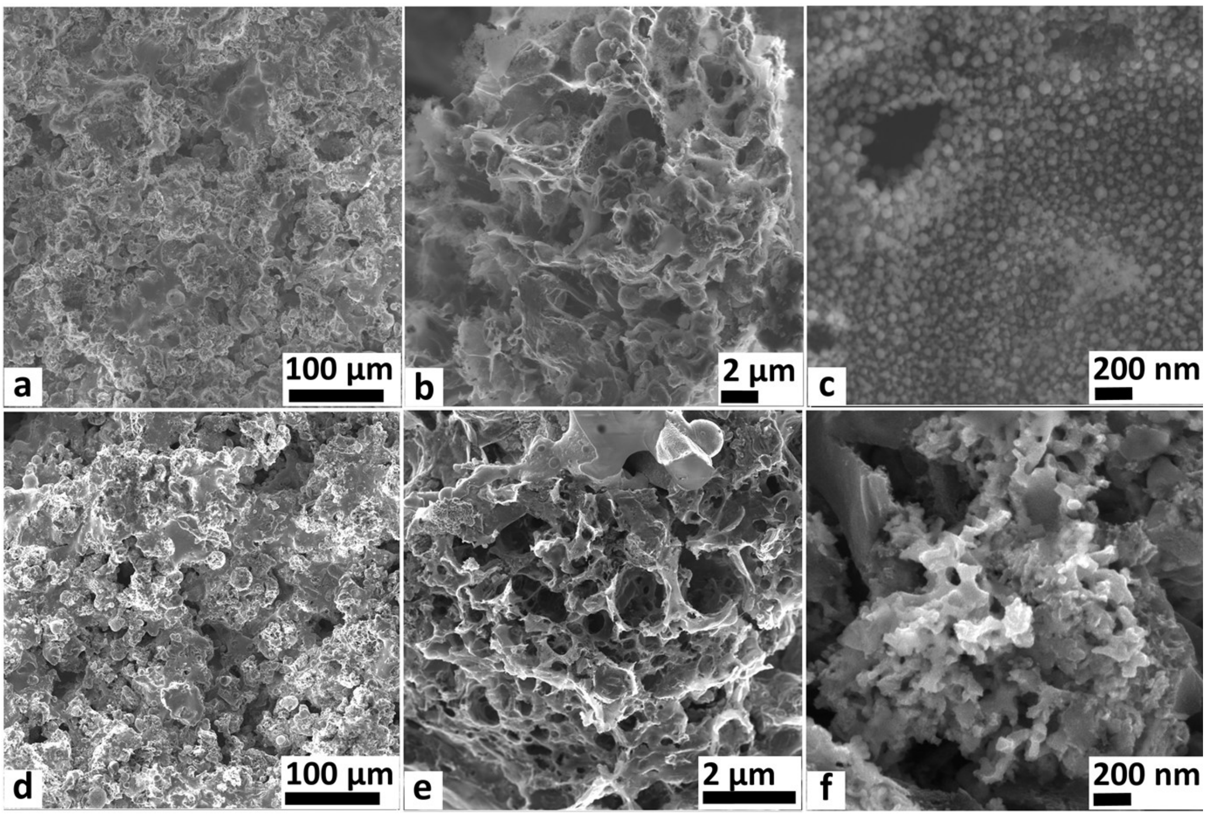

Figure S16. *SEM images of NiMo 16W@100mm (a-c) as-sprayed, and (d-f) after Al leaching.*

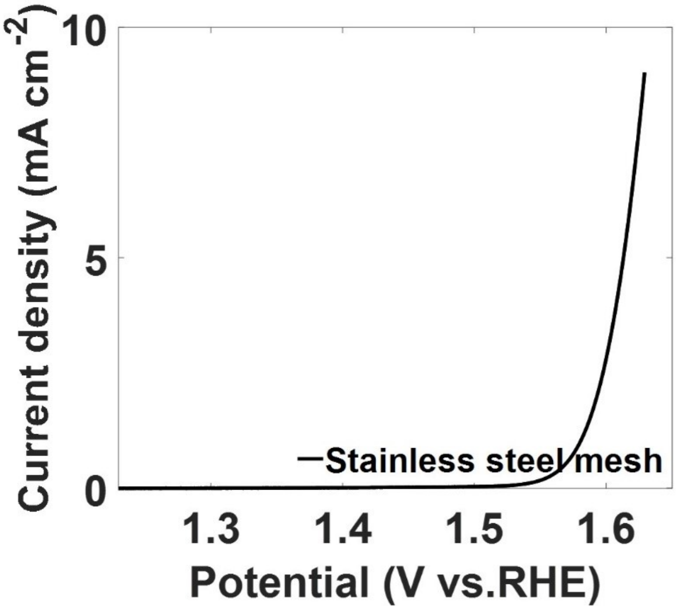

Figure S17. *Polarization curve of stainless-steel mesh in the potential range relevant for OER.*

References

1. Zhuang, Z., et al., *Nickel supported on nitrogen-doped carbon nanotubes as hydrogen oxidation reaction catalyst in alkaline electrolyte.* Nature Communications, 2016. **7**(1): p. 10141.
2. Bu, X., et al., *Remarkable gas bubble transport driven by capillary pressure in 3D printing-enabled anisotropic structures for efficient hydrogen evolution electrocatalysts.* Applied Catalysis B: Environmental, 2023. **320**: p. 121995.
3. Patil, R.B., et al., *Direct Observation of Ni–Mo Bimetallic Catalyst Formation via Thermal Reduction of Nickel Molybdate Nanorods.* ACS Catalysis, 2020. **10**(18): p. 10390-10398.
4. Liu, X., et al., *Identifying the Activity Origin of a Cobalt Single-Atom Catalyst for Hydrogen Evolution Using Supervised Learning.* Advanced Functional Materials, 2021. **31**(18): p. 2100547.
5. Zhou, B., et al., *Thermal oxidation–electroreduction modified 3D NiCu for efficient alkaline hydrogen evolution reaction.* International Journal of Hydrogen Energy, 2021. **46**(43): p. 22292-22302.
6. Wang, G., et al., *Trimetallic Mo–Ni–Co selenides nanorod electrocatalysts for highly-efficient and ultra-stable hydrogen evolution.* Nano Energy, 2020. **71**: p. 104637.
7. Zhang, K., et al., *Unveiling the synergy of polymorph heterointerface and sulfur vacancy in NiS/Ni3S2 electrocatalyst to promote alkaline hydrogen evolution reaction.* Applied Catalysis B: Environmental, 2023. **323**: p. 122144.

8. Wang, A., et al., *Flower-like MoS2 with stepped edge structure efficient for electrocatalysis of hydrogen and oxygen evolution.* International Journal of Hydrogen Energy, 2019. **44**(13): p. 6573-6581.
9. Lei, C., et al., *Nanostructured Carbon Based Heterogeneous Electrocatalysts for Oxygen Evolution Reaction in Alkaline Media.* ChemCatChem, 2019. **11**(24): p. 5855-5874.
10. Park, J.-H., J.C. Ro, and S.-J. Suh, *FeCo nanoparticles with different compositions as electrocatalysts for oxygen evolution reaction in alkaline solution.* Applied Surface Science, 2022. **589**: p. 153041.
11. Babar, P., et al., *Towards highly efficient and low-cost oxygen evolution reaction electrocatalysts: An effective method of electronic waste management by utilizing waste Cu cable wires.* Journal of Colloid and Interface Science, 2019. **537**: p. 43-49.
12. Ghosh, S., et al., *Inception of Co3O4 as Microstructural Support to Promote Alkaline Oxygen Evolution Reaction for Co0.85Se/Co9Se8 Network.* Inorganic Chemistry, 2020. **59**(23): p. 17326-17339.
13. Maruthapandian, V., et al., *Study of the Oxygen Evolution Reaction Catalytic Behavior of CoxNi1–xFe2O4 in Alkaline Medium.* ACS Applied Materials & Interfaces, 2017. **9**(15): p. 13132-13141.
14. Gond, R., et al., *Sodium Cobalt Metaphosphate as an Efficient Oxygen Evolution Reaction Catalyst in Alkaline Solution.* Angewandte Chemie International Edition, 2019. **58**(25): p. 8330-8335.